

Article

Preparation and Investigation of Sol–Gel TiO₂-NiO Films: Structural, Optical and Electrochromic Properties

Tatyana Ivanova ¹, Antoaneta Harizanova ^{1,*}, Tatyana Koutzarova ²  and Benedicte Vertruyen ³ 

¹ Central Laboratory of Solar Energy and New Energy Sources, Bulgarian Academy of Sciences, Tzarigradsko Chaussee 72, 1784 Sofia, Bulgaria; tativan@phys.bas.bg

² Institute of Electronics, Bulgarian Academy of Sciences, Tzarigradsko Chaussee 72, 1784 Sofia, Bulgaria; tatyana_koutzarova@yahoo.com or tanya@ie.bas.bg

³ GREENMAT, Institute of Chemistry B6, University of Liege, B6aQuartier Agora, Allee du Six Août 13, 4000 Liège, Belgium; b.vertruyen@ulg.ac.be

* Correspondence: tonyhari@phys.bas.bg

Abstract: TiO₂ and TiO₂-NiO films were successfully derived by a sol–gel dip coating technology. The impact of the thermal treatments (300–600 °C) on the structural, optical and electrochromic properties was investigated. X-ray diffraction (XRD) analysis showed that TiO₂ films were polycrystalline and evolved in the anatase phase. The composite TiO₂-NiO films, treated at annealing temperatures below 500 °C, contained anatase titania, a small inclusion of cubic NiO and an amorphous fraction. The formation of NiTiO₃ was exposed after the highest annealing at 600 °C. The presence of Ti-O-Ni bonds was determined in the composite films by Fourier-transform infrared (FTIR) spectroscopy. The optical properties and the optical band gap of TiO₂-NiO films were investigated and discussed. The transparency of the electrochromic TiO₂-NiO films was 76.8 and 78.3% in the 380–700 nm spectral range after film thermal treatments at 300 and 500 °C. NiO incorporation led to the narrowing of the optical band gap. The electrochromic (EC) properties of the composite films were improved compared to TiO₂ films. They had higher diffusion coefficients. Their color efficiencies are 37.6 (550 nm) and 52.2 cm²/C (600 nm).

Keywords: sol–gel; titanium dioxide; optical properties; electrochromic material



Citation: Ivanova, T.; Harizanova, A.; Koutzarova, T.; Vertruyen, B.

Preparation and Investigation of Sol–Gel TiO₂-NiO Films: Structural, Optical and Electrochromic Properties. *Crystals* **2024**, *14*, 192. <https://doi.org/10.3390/cryst14020192>

Academic Editor: Vladimir M. Kaganer

Received: 31 January 2024
Revised: 8 February 2024
Accepted: 12 February 2024
Published: 14 February 2024



Copyright: © 2024 by the authors. Licensee MDPI, Basel, Switzerland. This article is an open access article distributed under the terms and conditions of the Creative Commons Attribution (CC BY) license (<https://creativecommons.org/licenses/by/4.0/>).

1. Introduction

Titanium dioxide is known to be one of the most important semiconductors, attracting scientific research due to its chemical stability, non-toxicity and economical use [1,2]. TiO₂ possesses a high refractive index (above 2), high transparency and a large band gap [3]. TiO₂ thin films can exhibit different crystalline structures: amorphous, anatase, rutile and brookite phases. These phases determine their physical properties and corresponding applications. TiO₂ is studied for utilization in photocatalysis, gas sensors, self-cleaning coatings, antimicrobial surfaces, microelectronics, lithium ion batteries and solar cells [4,5]. Other interesting applications of TiO₂ are in semiconductor based photoelectrochemical water splitting or CO₂ reduction [1,6] and in electrochromic devices [7,8].

The electrochromic effect is described as a reversible modulation of the optical properties of certain materials upon an applied external voltage [9]. Based on the electrochemical double injection/extraction of small size ions (such as H⁺, Li⁺, Na⁺, and K⁺) and electrons, the electrochromic thin film is switched reversibly between the colored (absorbing) and bleached (transparent) states by applying weak negative and positive voltages [10]. Generally, an EC device is constructed from five layers: a transparent conducting oxide (TCO) layer, a cathodic electrochromic film, an ion-conducting layer (liquid, gel or solid), an anodic electrochromic film (or optically passive), and a TCO layer positioned between two substrates in a laminated configuration [11]. Electrochromic devices find an enormous range of practical applications including color displays, sensors, reflectance mirrors, vehicle

sunroofs, smart windows, rear-view mirrors, variable-emittance surfaces for temperature control of spacecraft, medical imaging detectors, and electrochromic paper [12,13].

TiO₂ is a cathodic electrochromic material, which changes its color to blue (absorbing state) upon small cation intercalation, and turns to the transparent (bleaching) state once the charge is deintercalated (extracted). The electrochromic effect can be described as follows: under the action of the electrical field applied onto the TiO₂ films/TCO substrate with a negative potential, the cations from the electrolyte are inserted into the film structure; and to compensate the charge, electrons (from TCO layer) are also injected. One of the most accepted mechanisms of electrochromic reactions is electron-ion double injection/extraction under the applied voltage into electrochromic functional material, TiO₂. This is described as follows [14,15]:



where TiO₂ is in transparent (oxidation) state and M_xTiO₂ is in colored (absorbing) state and M⁺ are either H⁺ or small ions, such as Li, Na, and K.

NiO is a well-known anodic electrochromic material, which colors (become absorbing—colored state) upon ion extraction and bleaches (transparent state) upon ion intercalation. NiO films have high optical modulation, good cycling reversibility, low cost, and a memory effect, but also show poor stability [16]. To enhance optical properties, electrochromic performance and stability, different ion dopants could be added in NiO [17,18]. NiO anodic electrochromic layers are promising materials as active counter electrodes in EC devices complementary to WO₃ [19,20].

The electrochromic effect in NiO films is complicated and is still under debate. It is proposed that the transition from the colored to bleached (absorbing) states is affected by the multiple valences of Ni ions in the NiO structure due to Ni 3d electrons [21]. The basic coloration electrochemical process of NiO electrodes in an aqueous alkaline solution can be written as [22]:



Throughout this electrochemical process, NiO films undergo reversible color modulation from the transparent to dark brown state. The electrochromic process involves dual injection or extraction of electrons and ions. A reduction process of Ni³⁺ to Ni²⁺ takes place during the cathodic scan and NiO film is bleached. In the reverse anodic scan, the oxidation process of Ni²⁺ to Ni³⁺ results in the coloration of the film.

In the electrochromic effect of NiO films in the case of anhydrous Li⁺-containing electrolytes, ion intercalation is proposed to proceed via two steps [23]. The first step involves irreversible insertion of Li⁺ in the NiO host structure. The second step includes the reversible intercalation/deintercalation process along with the electrochromic effect—the transparent/absorbing state [24]:



Mixing the two metal oxides is a technological approach to enhance and extend the properties of pure materials. Recently, TiO₂-NiO composite films are studied as enhanced electrochromic compounds and as solid electrodes in solar cells [25]. It has also been reported that Ni doping in TiO₂ films results in a smoother and more uniform surface as well as better photocatalytic properties [26]. The EC behavior of mixed TiO₂-NiO films improves cycling stability and enhances the transmittance contrast for visible and near-IR light EC devices [27].

Combining anodic and cathodic electrochromic metal oxides, the resulting type of electrochromic response is strongly dependent on the ratio of the two components. Ni-W oxide is a mixed electrochromic material and it is well studied [28,29]. Increasing the tungsten component, the electrochromic process with Li⁺ ions is cathodic as established

for WO_3 [30]. For NiO-TiO_2 with higher Ni molar concentrations, the electrochromism is anodic [31].

This paper presents the sol-gel preparation of the composite TiO_2 - NiO films. The aim is to determine the impact of Ni addition on the optical and electrochromic behavior of TiO_2 films. The structural, optical and electrochromic properties of the obtained nanostructured films are investigated in terms of thermal treatments. TiO_2 and TiO_2 - NiO films are successfully obtained by the sol-gel technology using the dip coating method on different substrates: Si, glass and glass covered with SnO_2 :Sb layer substrates. XRD, FTIR spectroscopy, UV-VIS spectrophotometry and cyclic voltammetry are applied to characterize TiO_2 and TiO_2 - NiO films after annealing at temperatures from 300 to 600 °C.

2. Materials and Methods

2.1. Thin Film Preparation

Sol solution synthesis for depositing TiO_2 films was reported in detail in [32]. The precursor used was tetraethyl orthotitanate (>97% purity, Fluka Chemie, Buchs, Germany). The addition of 1.5 M glacial acetic acid (100%, Merck KgaA, Darmstadt, Germany) caused acetate modification. Further, the solution was adjusted by inserting a certain amount of water, causing hydrolysis and condensation reactions. The solution was converted to a gel. The 1 M acetylacetone (>98%, Sigma Aldrich Chemie, Buchs, Germany) was applied as a peptizing agent and a stabilizer. Absolute ethanol (Merck KgaA, Darmstadt, Germany) was used as a solvent. The solution became transparent after aging 1 week without precipitation. It must be noted that the synthesized sol solution for obtaining TiO_2 films was verified to be stable for more than 1 year, maintaining its excellent film-forming properties. The precursor of the Ni additive was nickel chloride ($\text{NiCl}_2 \cdot 6\text{H}_2\text{O}$, 98 +%, Merck KgaA, Darmstadt, Germany). The appropriate amount of NiCl_2 was introduced in the prepared TiO_2 sol in order to obtain a TiO_2 -0.5 NiO system in molar parts. The mixed sol solution was stirred on a magnetic stirrer for 1 h, then ultrasonically treated at 40 °C/30 min. The Ti-Ni solution was homogenous and transparent.

Different substrates were used: silicon wafers (FZ, p-type, resistivity 4.5–7.5 Ω , orientation <100>, diameter 25.4 mm), ordinary glass (size 78 × 25 mm) and conductive glass substrates (glass covered with SnO_2 :Sb layer, size 70 × 25 mm, sheet resistance 15 Ω /sq). The substrates were cleaned just before film deposition. Si wafers were applied for structural and vibrational studies, the glass for optical characterization and the conductive glass substrates for electrochromic properties.

TiO_2 and TiO_2 - NiO thin films were obtained by immersing the substrates in the corresponding sols. Then, they are withdrawn with a withdrawal speed of 10 $\text{cm} \cdot \text{min}^{-1}$ (dip coating process). The preheating temperature, chosen to eliminate the organics from the as-deposited coatings was 300 °C for 30 min. The coating and preheating treatments were repeated three times. The obtained sol-gel films were finally subjected to high annealing at temperatures of 300, 400, 500 and 600 °C for 1 h in ambient air. The preheating and the annealing treatments were carried out in a chamber furnace with controllable heating and a cooling rate of 10 °C/minute. This technological approach enables obtaining very uniform and homogeneous TiO_2 and mixed TiO_2 - NiO thin films.

2.2. Thin Film Characterization Techniques

X-ray diffraction (XRD) patterns were taken by a XRD diffractometer Bruker D8 (Bruker AXS GmbH, Karlsruhe, Germany), using $\text{Cu K}\alpha$ radiation with a wavelength of 1.54056 Å in the scan range $2\theta = 20$ – 70° , with a grazing incidence angle of 2° and a step time of 8 s. FTIR measurements were recorded by using Shimadzu FTIR Spectrophotometer IRPrestige-21 (Shimadzu Corporation, Kyoto, Japan) in the spectral range 350–4000 cm^{-1} . A bare Si wafer was employed as background. Optical characterization was performed with a UV-VIS-NIR Shimadzu 3600 double-beam spectrophotometer (Shimadzu Corporation, Kyoto, Japan) in the spectral region of 280–1800 nm. The transmittance spectra of the samples were taken against air. The reflectance spectra were measured by using the

specular reflectance attachment (5° incidence angle) and an Al-coated mirror as references. Film thickness was measured with a LEF 3 M laser ellipsometer (Siberian Branch of the Russian Academy of Sciences, Novosibirsk, Russia), using a He-Ne laser (wavelength of 632.8 nm).

2.3. Cyclic Voltammetry Set up and Electrochromic Characteristics

Electrochromic behavior was investigated by means of cyclic voltammetry. The measurements were performed in a standard three-electrode cell arrangement, using a Pt wire as the counter electrode. The reference electrode was a saturated calomel electrode (SCE). The used electrolyte was 1 M LiClO₄ (Fluka Chemie, Buchs, Germany) in propylene carbonate (PC, Merck KgaA, Darmstadt, Germany) (1 M LiClO₄+PC). The voltage sweep potentials were provided by a computer-controlled Bank-Elektronik Potentiostat (Bank Elektronik—Intelligent Controls GmbH, Pohlheim, Germany).

For estimating color change, the equipment was upgraded with an optical system, consisting of a chipped light source, a monochromator and a lock-in amplifier. The signal has been automatically measured as a function of the applied voltage. An IR-LED and a second photodetector provided a reference signal for the lock-in amplifier. The signal change was controlled by an oscilloscope. This cyclic voltammetry set up enables simultaneously measuring the current, the charge and the transmittance change as a function of the applied voltage. The applied voltage varied from -2 V to $+1$ V. The voltammograms were measured using different scan rates in the range of 10–50 mV/s.

Color efficiency (CE) is an electrochromic characteristic that qualifies the modulation of the optical properties of electrochromic material. The CE characteristic is an important indicator for the applications and fabrication of electrochromic electrodes. CE is defined as follows [33]:

$$CE = \frac{\Delta OD}{Q} \quad (6)$$

where ΔOD is the optical density and ΔQ is the injected/ejected electronic charge.

Experimentally, the optical density, ΔOD , is estimated from the expression:

$$\Delta OD = -\log_{10}\left(\frac{T_{bleached}}{T_{colored}}\right) \quad (7)$$

where $T_{bleached}$ and $T_{colored}$ are the transmittance in the bleached state and in the colored state, respectively. The color efficiency is spectrally dependent so a comparison is acceptable only for the CE values determined for a certain wavelength or spectral range.

3. Results

3.1. The XRD Study

The XRD patterns of the TiO₂ and TiO₂-NiO films annealed at 400–600 °C are presented in Figure 1. The most intense diffraction peaks in the diffractogram of the pure TiO₂ film treated at 400 °C (Figure 1a, black curve) correspond to the tetragonal anatase phase (according to PDF 01-071-1166). The intensity of the (112) anatase reflection is higher than would be expected for a random powder pattern. This could be due to a preferential orientation of crystallization, but there are two weak unindexed reflections, marked by * symbols. These two reflections (at 44.7° and 65.1°) and the reflection at the position of the (112) reflection of anatase (38.4°) have similar peak widths and they all display a higher intensity in the TiO₂-NiO film annealed at 400 °C (Figure 1a, pink curve), suggesting that they could belong to an unidentified intermediate phase. The annealing at 500 °C of the sol-gel TiO₂ film results in anatase titanium dioxide without other crystal phases (Figure 1b, black curve); in agreement with the reference pattern of anatase, the (004) reflection at 37.3° degrees is more intense than the (112) reflection at 38.4° . The highest annealing temperature (600 °C) induces the emergence of weak peaks located at 27.4 , 54.5 and 56.5° (Figure 1c, black curve), which correspond to the rutile TiO₂ phase (PDF 01-089-0552). The crystallite sizes in the TiO₂ films were estimated using the Scherrer equation, considering the (101)

reflection of the anatase phase (25.4°). The crystallites grow larger with an increase in the annealing temperature. The determined values are 10 nm (after annealing at 400°C), 13 nm (at 500°C) and 23 nm (at 600°C).

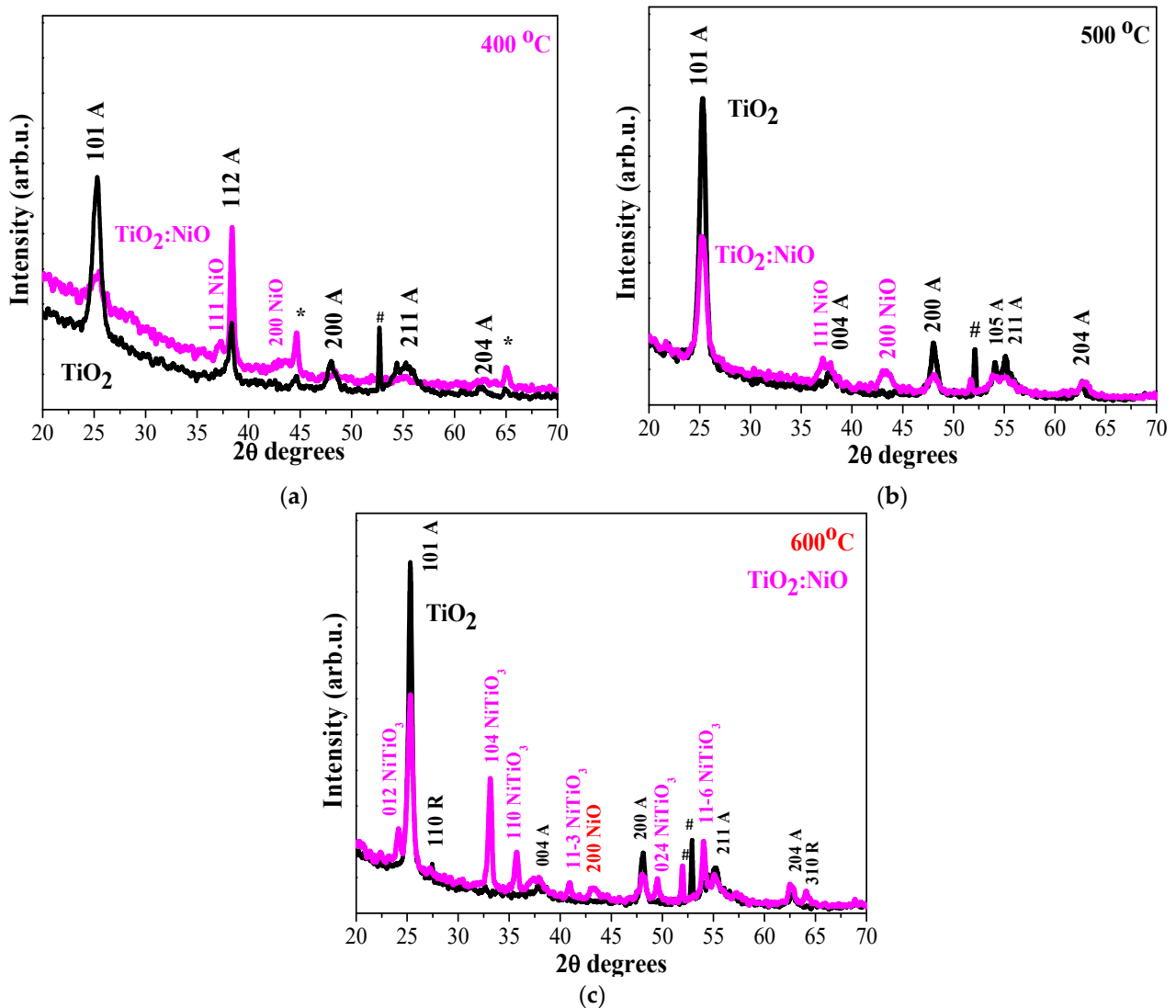


Figure 1. XRD patterns of the sol-gel TiO_2 films (in black) and TiO_2 -NiO films (in pink) annealed at temperatures of (a) 400°C , (b) 500°C and (c) 600°C . The reflections of the anatase (A), rutile (R), NiO and NiTiO_3 phases are labelled with their hkl indices. The unindexed peaks labeled with * symbols are discussed in the main text. Peaks attributed to the Si substrate are marked by # symbols.

The XRD pattern of the mixed oxide film annealed at 400°C (Figure 1a, pink curve) shows a broader and less intense (101) anatase reflection than in the case of the pure TiO_2 film. The most intense reflection is the one at the position of the (112) reflection of anatase, followed by the two unindexed peaks marked with a * symbol. Weak and broad peaks of cubic NiO are also observed at 37.2 and 43.4° (PDF 00-047-1049). In the XRD pattern of the mixed oxide film annealed at 500°C (Figure 1b, pink curve), the two reflections attributed to cubic NiO are still weak and broad. The main phase is anatase with an estimated crystallite size of 9 nm, compared to 13 nm for the pure TiO_2 film. The results at 400 and 500°C lead to the conclusion that Ni incorporation delays the film crystallization and the crystallite growth, and is accompanied by the segregation of a NiO fraction.

The reflections in the XRD pattern of the TiO_2 -NiO film annealed at 600°C (Figure 1c, pink curve) can be assigned to four crystal phases: anatase TiO_2 , rhombohedral NiTiO_3 , traces of cubic NiO and traces of rutile TiO_2 . The peaks at 24.20° , 33.1° , 35.7° , 40.9° , 49.5°

and 54.1° correspond to the NiTiO_3 phase in accordance with PDF 03-010-7290. The estimated crystallite sizes of anatase and NiTiO_3 were 19 nm ((101) reflection) and 29 nm ((104) reflection), respectively. The appearance of NiTiO_3 in mixed oxide films was previously reported by others [34]. NiTiO_3 is studied for its applications in electronics, photoemission, photocatalysis and sensors [35]. It crystallizes with the ilmenite structure [36]. There are some reports of the multiferroic properties of NiTiO_3 , which potentially enable switching of the direction of magnetization by applying an electric field [37].

It can be concluded from the XRD analysis that the sol-gel TiO_2 films are polycrystalline with the predominant anatase phase in the studied annealing temperatures. The addition of nickel tends to delay the crystallization of the TiO_2 phase, with a minor segregation of the cubic NiO phase at $400^\circ\text{C}/500^\circ\text{C}$ and the appearance of rhombohedral NiTiO_3 at 600°C .

3.2. FTIR Spectroscopy

FTIR spectroscopy is used for characterizing the vibrational properties of TiO_2 and $\text{TiO}_2\text{-NiO}$ films. The structural and functional data about the sample analyzed can be obtained from the absorption bands, their shifting, the change in their intensities and shapes in the recorded spectra. FTIR spectra of annealed TiO_2 and $\text{TiO}_2\text{-NiO}$ films are presented in Figure 2.

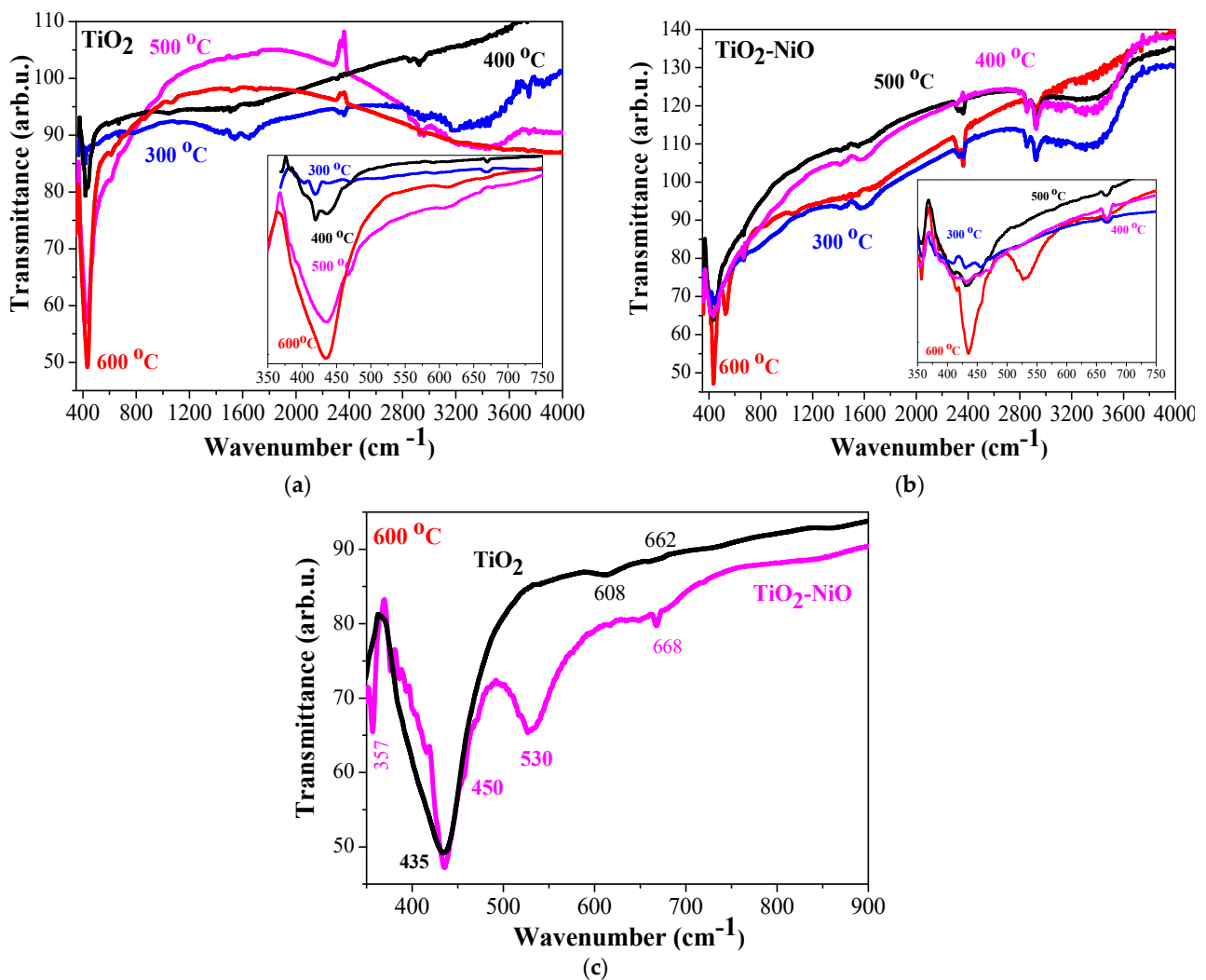


Figure 2. FTIR spectra of (a) sol-gel TiO_2 , (b) $\text{TiO}_2\text{-NiO}$ films annealed at $300\text{--}600^\circ\text{C}$, where the inserted figures present the spectra in the range $350\text{--}750\text{ cm}^{-1}$, and (c) the comparison of TiO_2 and $\text{TiO}_2\text{-NiO}$ films, treated at 600°C in the spectral range $350\text{--}900\text{ cm}^{-1}$.

The observed bands above 1100 cm^{-1} are due to the organic residues, resulting from the sol–gel process. FTIR spectra reveal absorption bands at 3400 and at 1600 cm^{-1} , which are attributed to the stretching modes and the bending vibrations of hydroxyl groups, respectively [4]. These absorption features are more well expressed for TiO_2 -NiO films. The water present can be as a result of the sol–gel deposition or of the water adsorption from the environmental moisture. These absorption bands vanish after annealing at the highest temperature, $600\text{ }^\circ\text{C}$. The vibrations of C-H bonds are observed at 2930 and 2855 cm^{-1} (in the spectra of TiO_2 and TiO_2 -NiO films) [38]. The absorption band at 2360 cm^{-1} is assigned to the C-O vibrations due to the atmospheric CO_2 as FTIR measurements are carried out in air [39]. The absorption at approximately 1500 cm^{-1} is associated with the asymmetric stretching vibrations of O=C-O bonding and it was found to be stable even after high-temperature annealing [40].

The infrared absorption features below 1000 cm^{-1} are characteristic of metal–oxygen bonds. The band at approximately 668 cm^{-1} , in all spectra, can be assigned to Ti-O-Ti bridges of anatase titania [40]. TiO_2 film, annealed at $300\text{ }^\circ\text{C}$ (Figure 2a), displays weak absorption bands at 590 and 462 cm^{-1} , which are related to the lattice vibration of anatase TiO_2 [40] and the stretching vibrations of Ti-O bonds, respectively. The main absorption band is split into two bands at 419 and 438 cm^{-1} . These bands are associated with Ti-O stretching vibrations. In fact, the band at 438 cm^{-1} is associated with the fundamental Ti-O stretching mode of anatase [41]. TiO_2 -NiO films, treated at $300\text{ }^\circ\text{C}$, have IR absorption features at 670 , 456 , 430 , 405 and 360 cm^{-1} . It is seen that the addition of NiO changes the vibrational properties. The new band positioned at 456 cm^{-1} is attributed to the formation of Ti-O-Ni bonds [42].

The two bands observed at 405 and 430 cm^{-1} are related to the Ti-O stretching modes [43]. Increasing the annealing temperature up to $400\text{ }^\circ\text{C}$ results in increasing the intensities of the main absorption bands, signaling the beginning of crystallization. IR bands in the FTIR spectrum of TiO_2 are characteristic of anatase titania. The absorption bands in the TiO_2 -NiO spectrum can be assigned to anatase and Ti-O-Ni bonds. A new weak band at 514 cm^{-1} (TiO_2 -NiO spectrum) is related to Ni-O bond vibrations [44]. After the thermal treatment at $500\text{ }^\circ\text{C}$, all IR absorptions in the spectrum of TiO_2 film are mainly attributed to the anatase phase and the main absorption band is stronger. In the case of TiO_2 -NiO films, a new weak feature at 470 cm^{-1} is present, which is due to Ni-O bonding [44]. All the other observed absorption bands are assigned to anatase titania.

There are interesting absorption features in the spectra of the studied films after the highest annealing temperature of $600\text{ }^\circ\text{C}$. The TiO_2 -NiO film spectrum has a shoulder at 412 cm^{-1} (due to rutile TiO_2), a very strong band at 435 cm^{-1} characteristic of anatase TiO_2 , and a broad strong band centered at 530 cm^{-1} (509 – 550 cm^{-1}), which is most probably connected to the Ni oxide fraction. IR bands in this spectral range are reported as an indication for the existence of NiTiO_3 [45]. The observed bands at 530 cm^{-1} , the shoulder at 450 cm^{-1} , and the band at 357 cm^{-1} have been assigned to nanocrystalline NiTiO_3 [46,47].

FTIR analysis supports the findings from the XRD study that the NiO fraction exists in TiO_2 -NiO films annealed at lower temperatures of 300 – $500\text{ }^\circ\text{C}$. The formation of nickel titanate is shown after the highest-temperature treatment at $600\text{ }^\circ\text{C}$. The composite film structure becomes more complicated with the appearance of more phases: anatase and rutile TiO_2 , nickel titanate (NiTiO_3) and NiO.

3.3. Optical Properties

Transmittance and reflectance spectra are measured for the sol–gel TiO_2 and TiO_2 -NiO films, deposited on glass and conductive glass substrates. Figure 3 presents the optical spectra of TiO_2 and mixed TiO_2 -NiO films annealed at 300 , 500 and $600\text{ }^\circ\text{C}$ and deposited on glass substrates.

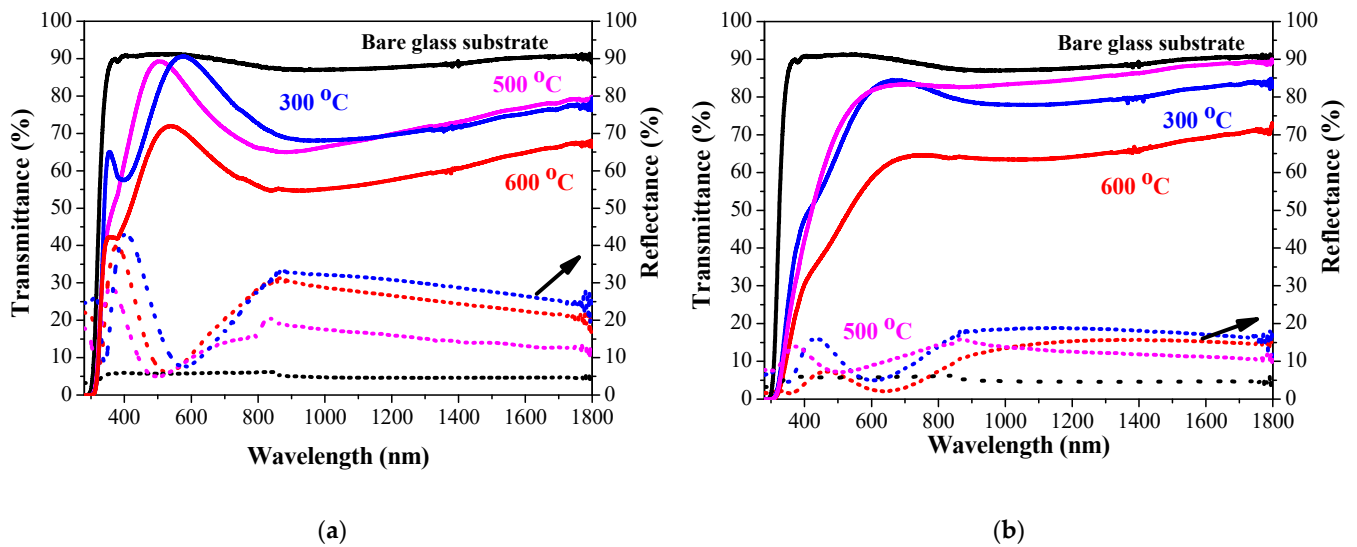


Figure 3. Transmittance and reflectance spectra of sol-gel (a) TiO_2 and (b) $\text{TiO}_2\text{-NiO}$ films, deposited on glass and thermally treated at 300, 500 and 600 °C. The corresponding spectra of bare glass substrates are given as references. Solid lines present transmittance and dotted lines present reflectance.

Transmittance and reflectance spectra of bare glass substrate are given as references. The spectra are taken against air. The average transmittance and reflectance values (for visible spectral range 450–750 nm) of the studied films are estimated and given in Table 1. The best transparency is observed for TiO_2 annealed at 300 °C— T_{average} is 83.1%. It can be seen that TiO_2 films (Figure 3a) exhibit the lowest transmittance after annealing at 600 °C. The highest reflectance is observed for TiO_2 films annealed at 300 °C, 14.4%. Increasing the annealing temperature results in lowering the reflectance. Similar optical behavior is found for the mixed oxide films. $\text{TiO}_2\text{-NiO}$ films annealed at 300 and 500 °, show an average transmittance of 76.8 and 78.3% in the spectral range 450–750 nm. The transparency is sharply diminished after 600 °C thermal treatment. The average reflectance of the composite films is below 10% for all the samples (see Table 1).

Table 1. The average transmittance (T_{average}) and reflectance (R_{average}) of sol-gel TiO_2 and $\text{TiO}_2\text{-NiO}$ film in the spectral range 450–750 nm, depending on the annealing temperature. The used substrates are glass and conductive glass.

	Annealing Temperature (°C)	Glass *		Conductive Glass #	
		T_{average} (%)	R_{average} (%)	T_{average} (%)	R_{average} (%)
TiO_2	300	83.1	15.2		
	500	79.9	9.8	76.3	19.5
	600	65.8	13.5		
$\text{TiO}_2\text{-NiO}$	300	76.8	8.2	68.7	7.7
	500	78.3	9.3	62.3	7.3
	600	55.5	4.1		

* Bare glass substrate: $T_{\text{average}} = 90.5\%$ and $R_{\text{average}} = 5.8\%$. # Bare conductive glass: $T_{\text{average}} = 81.0\%$ and $R_{\text{average}} = 10.2\%$.

It has been found that pure TiO_2 films are more transparent than $\text{TiO}_2\text{-NiO}$ films. This can be related to the multiphase structure of the composite films, inducing structural defects and disorder. An increase in light scattering and absorption of the composite films is expected.

Figure 4a exhibits UV–VIS spectra of $\text{TiO}_2\text{-NiO}$ films, treated at 300 and 500 °C and deposited on the conductive substrates, together with the corresponding spectra of the

bare conductive glass. It is observed that increasing the annealing temperature results in lower film transparency. A comparison of the transmittance and the reflectance spectra of TiO₂ and TiO₂-NiO films annealed at 500 °C and deposited on conductive glass is shown in Figure 4b. The transmittance of TiO₂ films is better than the transparency of TiO₂-NiO films, as has been observed for ordinary glass substrates. The Tauc relation is employed to estimate the optical band gap of the sol-gel films [48]:

$$(\alpha h\nu) = B (h\nu - E_g)^m \quad (8)$$

where 'B' is a constant, h is Plank's constant, ν is the photon frequency, α is the absorption coefficient and E_g is the optical band gap. The constant m is the power factor characterizing the nature of electronic transitions between the valence band and the conduction band. It can take the following values: 1/2 for allowed direct, 2 for allowed indirect, 3 for forbidden direct and 3/2 for forbidden indirect optical transitions.

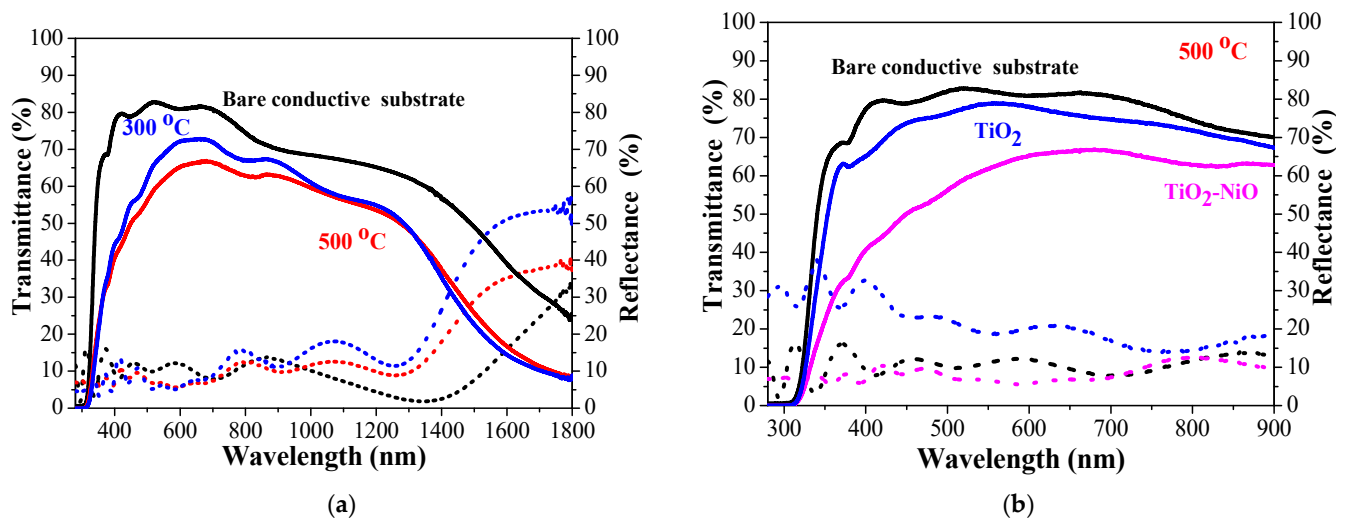


Figure 4. Transmittance and reflectance spectra of (a) TiO₂-NiO films, deposited on conductive glass and thermally treated at 300 and 500 °C and (b) the comparison of the optical spectra of TiO₂ and TiO₂-NiO films annealed at 500 °C. Solid lines present transmittance and dotted lines present reflectance.

The absorption coefficient, α , has been estimated by using the film thickness, d , the transmittance, T , and the reflectance, R [48]:

$$\alpha = -\frac{1}{d} \ln \left(\frac{(1-R)^2}{T} \right) \quad (9)$$

The film thickness of TiO₂ and TiO₂-NiO films is found to be comparable. The samples annealed at 300 °C are 120 nm thick. After thermal treatments at 500 and 600 °C, the film thickness is 100 nm.

It has been established that TiO₂ has direct and indirect band gaps [49,50]. The indirect and direct band gap of the sol-gel deposited films are determined by plotting $(\alpha h\nu)^{1/2}$ vs. $h\nu$ and $(\alpha h\nu)^2$ vs. $h\nu$ curves and by extrapolating the linear portion of the graphs to the energy axis, respectively.

Sol-gel deposition requires annealing procedures. Usually, the heat treatment decreases the film thickness and results in a denser structure due to the evaporation of the solvents and the removal of the residual organic groups or organic compounds [51]. Our previous study [52] of the sol-gel spin-coated TiO₂-V₂O₅ films reveals the same tendency. The film thickness and the film porosity decrease with increasing annealing temperatures [52].

The determined direct and the indirect optical band gaps of the studied sol–gel films obtained on the glass substrates are presented in Figure 5. As can be seen, the indirect optical band gaps are smaller than that of the direct gap values. TiO₂ films have direct E_g values ranging from 3.96 to 3.89 eV, slightly narrowing with increasing annealing temperatures. The corresponding indirect optical band gaps vary from 3.80 to 3.59 eV. TiO₂-NiO films were found to possess smaller values for optical band gaps, as shown in Figure 5. The E_g of TiO₂-NiO films are 3.86–3.81 eV (direct) and 3.58–3.32 eV (indirect), varying with the annealing temperature. The optical band gaps are significantly narrowed after annealing at the highest temperature, 600 °C. Similar behavior of the narrowing of the optical band gap with annealing was previously reported [53]. This effect could be related with the structural modifications, increasing the crystallite sizes and the variation in the film density. The sharp drop in the optical band gaps (direct and indirect) after the highest annealing at 600 °C can also be connected to the inclusion of the rutile phase (in the case of TiO₂ films) and with the presence of the NiTiO₃ phase and the traces of rutile titania in the composite film structure of TiO₂-NiO. It is well known that the rutile TiO₂ structure has a direct band gap of 3.06 eV and an indirect band gap of 3.10 eV [54]. On the other hand, for NiTiO₃, lower optical band gaps are reported: direct E_g = 2.7–3.1 eV [55,56] and indirect E_g = 2.02–2.62 eV [56,57]. The obtained optical band gaps of TiO₂ and TiO₂-NiO films are in good agreement with the reported values in the literature [57,58].

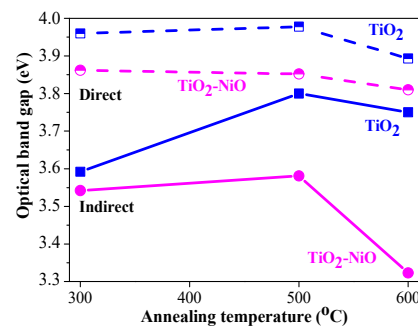


Figure 5. Optical band gap (E_g) values (direct and indirect) of TiO₂ and TiO₂-NiO films, depending on the annealing temperature. Solid lines present indirect E_g and dotted lines present direct E_g.

The optical constants, extinction (k) and refractive (n) coefficients of sol–gel TiO₂ and TiO₂-NiO films are estimated from the spectrophotometric data [48]:

$$k = \frac{\alpha\lambda}{4\pi} \quad (10)$$

$$n = \frac{1 + R}{1 - R} + \sqrt{\frac{4R}{(1 - R)^2} - k^2} \quad (11)$$

where α is the calculated absorption coefficient, λ is wavelength of radiation and R is the measured reflectance.

Figure 6 exhibits the results of optical constant determination dependent on the annealing temperature. The extinction coefficient is strongly affected by the annealing temperature. Its values are highest for the thermal treatment at 600 °C. The refractive index dispersions of the sol–gel TiO₂ and TiO₂-NiO films (Figure 6b) show some peaks in the spectral range 388–418 nm (for the titanium dioxide films) and 370–465 nm for the composite samples. The intensity of these refractive index peaks decrease with annealing temperatures. These features can be due to the defects in the film structure and the material stoichiometry [59]. The inset figures in Figure 6b show the refractive index values in the visible spectral range. It can be observed that the sol–gel dip-coated TiO₂ films have refractive index values between 1.58 and 1.85 at a wavelength of 550 nm and 1.88–2.18 at 632.8 nm and the corresponding data for TiO₂-NiO films is 1.61–1.77 at 550 nm and 1.43–1.92 at 632.8 nm (see Table 2). The refractive index of TiO₂ films is lower than the

characteristic value of 2.52 for anatase bulk titania, and this can be due to structural defects and the presence of an amorphous phase [60]. The obtained results for the refractive index are in an agreement with the reported refractive index of TiO₂ films, deposited by different methods [59–62]. The composite films have smaller refractive index values than TiO₂ films after annealing at 300 °C and 500 °C. The tendency is reversed for the samples treated at the highest temperature.

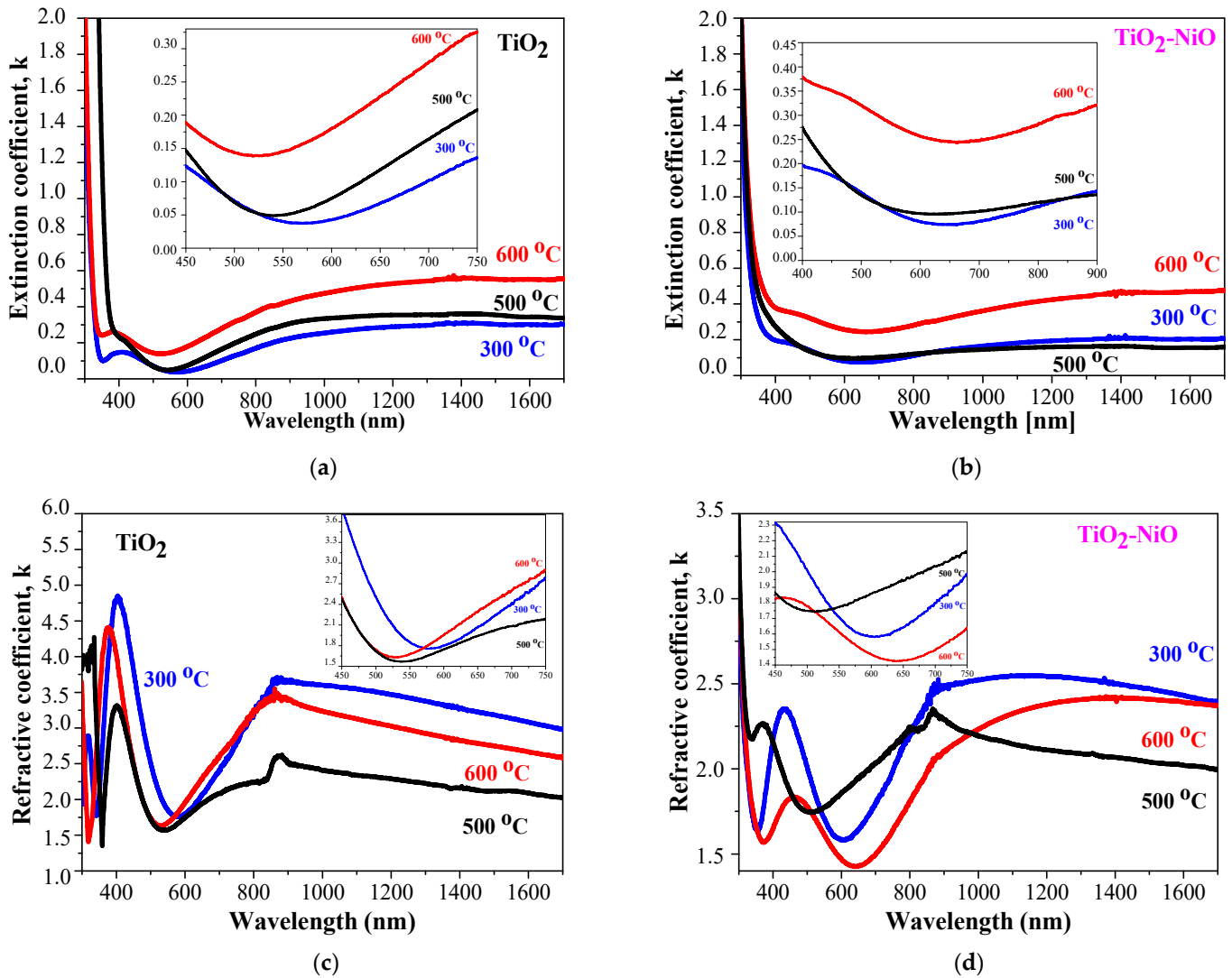


Figure 6. The extinction coefficient (*k*) of (a) TiO₂ and (b) TiO₂-NiO films and the refractive index (*n*) of (c) TiO₂ and (d) TiO₂-NiO films, depending on the annealing temperature. The inserted figures shows the *k* and *n* values in the visible spectral range 450–750 nm.

Table 2. The refractive index and porosity of sol-gel TiO₂ and TiO₂-NiO films on glass substrate.

	<i>T</i> _{annealing} (°C)	<i>n</i> , λ = 550 nm	<i>n</i> , λ = 632.8 nm	Porosity [%]
TiO ₂	300	1.85	1.95	55.8
	500	1.58	2.18	40.8
	600	1.67	1.88	60.2
TiO ₂ -NiO	300	1.70	1.60	75.4
	500	1.61	1.43	83.5
	600	1.77	1.91	58.2

XRD analysis determines that the composite films have lower crystallinity at an annealing temperatures below 500 °C and the presence of the NiO fraction. After annealing

at 600 °C, there is a mixture of several phases: anatase, rutile, NiO, and NiTiO₃. The refractive index of the amorphous material is smaller than that of the crystalline phase [63]. For NiO bulk, $n = 2.1818$ [63]. NiO films are reported to have a refractive index of 1.871 [63], 1.55–1.65 [64] and approximately 1.9 [60] at 550 nm. The refractive index of NiTiO₃ is 2.42 (at 632.8 nm) [65]. TiO₂-NiO films have a higher refractive index than pure TiO₂ due to the presence of the nickel titanate, rutile titania and nickel oxide crystalline phases.

The porosity of TiO₂ and TiO₂-NiO films is estimated from the following equation [60]:

$$Porosity = \left(1 - \frac{n^2 - 1}{n_o^2 - 1}\right) \times 100 (\%) \quad (12)$$

where n is the calculated refractive index at a wavelength of 632.8 nm and n_o is the bulk value 2.52. The obtained porosity results are given in Table 2.

The porosity of the composite films is higher for the samples treated at annealing temperatures of 300 and 500 °C. The porosity values after annealing at 600 °C are closed for TiO₂ and TiO₂-NiO films. As the electrochromic process is associated with the double injection (extraction) of ions and electrons to (from) the thin film structure, the porosity can enhance this process. TiO₂ and TiO₂-NiO films are transparent in the visible spectral range. The annealing treatment at 600 °C causes a decrease in film transmittance. Higher transparency is obtained for the sol-gel films treated at lower temperatures up to 500 °C. The studied sol-gel films have optical properties suitable for electrochromic applications.

3.4. Electrochromic Investigation

Electrochromic characterization is performed by voltametric measurements. The electrolyte used is 1 M LiClO₄ + PC. Different scan rates are applied. Figure 7 shows the cyclic voltammograms (CVs) of the pure TiO₂ and mixed TiO₂-NiO films treated at 300 °C. Stability testing was performed for up to 1200 cycles at a scan rate of 10 mV/s. TiO₂ and TiO₂-NiO retained their electrochromic properties during testing.

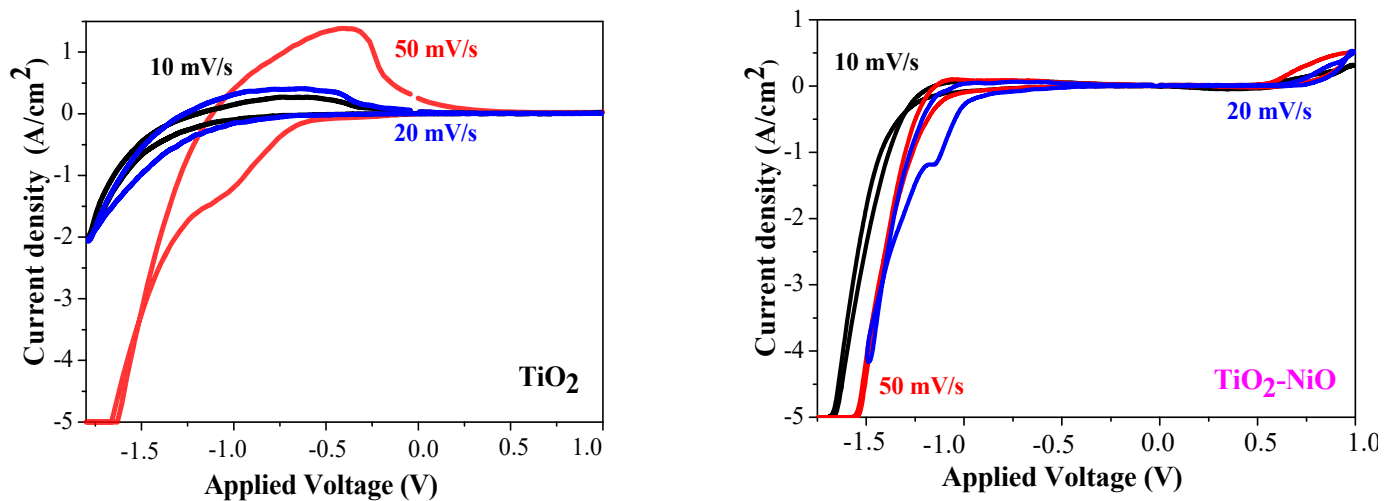


Figure 7. Cyclic voltametric curves of TiO₂ and TiO₂-NiO films, recorded at scan rates of 10, 20 and 50 mV/s. The films are annealed at 300 °C for 1 h.

The diffusion coefficient (D) of Li⁺ ions during intercalation and deintercalation is calculated by using the Randles–Sevcik equation [66]:

$$i_p = 2.72 \times 10^{-5} \times n^{3/2} \times D^{1/2} \times C_o \times v^{1/2} \quad (13)$$

where i_p is the peak current density (A/cm²), n is the number of electrons per reaction species (it is 1 for Li⁺), C_o is the concentration of active ions in the solution (mol/cm³),

and ν is the scan rate (V/s). The peak current density is determined from the CV curves (Figure 7).

Table 3 presents the obtained results for the diffusion coefficient, D_{Li} , and for the electrochromic characteristics: the optical modulation, ΔT , and the color efficiency, CE , estimated for a wavelength of 600 nm.

Table 3. The peak current density, i_p , the diffusion coefficient, D_{Li} , the optical modulation, ΔT , and the color efficiency, CE , of sol-gel TiO₂ and TiO₂-NiO film at different scan rates, ν . The films are annealed at 300 °C/1 h. The electrochromic characteristics are estimated for $\lambda = 600$ nm.

	ν (mV/s)	i_p (A/cm ²)	D_{Li} (cm ² /s)	ΔT (%)	CE (cm ² /C)
TiO ₂	10	0.27	9.85×10^{-10}	12.78	9.54
	20	0.44	13.08×10^{-10}	20.21	22.06
	50	1.42	54.50×10^{-10}	13.20	13.59
TiO ₂ -NiO	10	0.03	0.12×10^{-10}	25.29	40.71
	20	0.05	0.17×10^{-10}	31.23	52.17
	50	0.09	0.22×10^{-10}	6.59	9.51

It was found that the peak current density is dependent on the scan rate as expected from the Randles–Sevcik equation. A linear dependence of i_p vs. $\nu^{1/2}$ is determined, especially for TiO₂-NiO films. This is evidence for the chemically reversible redox process [67]. The mixed oxide films have higher diffusion coefficients in respect to TiO₂ films. The diffusion coefficients for Li⁺ ions are reported to be in the range of 0.35×10^{-10} – 2.46×10^{-10} cm²/s for the sol-gel TiO₂ films [68] and from 1×10^{-11} up to 4×10^{-10} cm²/s for MOCVD TiO₂ films [66].

The electrochromic characteristics are dependent on the scan rates. The highest optical modulation (ΔT) and color efficiency (CE) are obtained at a scan rate of 20 mV/s. Based on these results, other electrochemical experiments have been carried out at this scan rate. TiO₂ films treated at 300, 400 and 500 °C have been electrochemically measured and their electrochromic characteristics were estimated. Figure 8 presents the optical modulation and the color efficiency values in the spectral range of 450–850 nm.

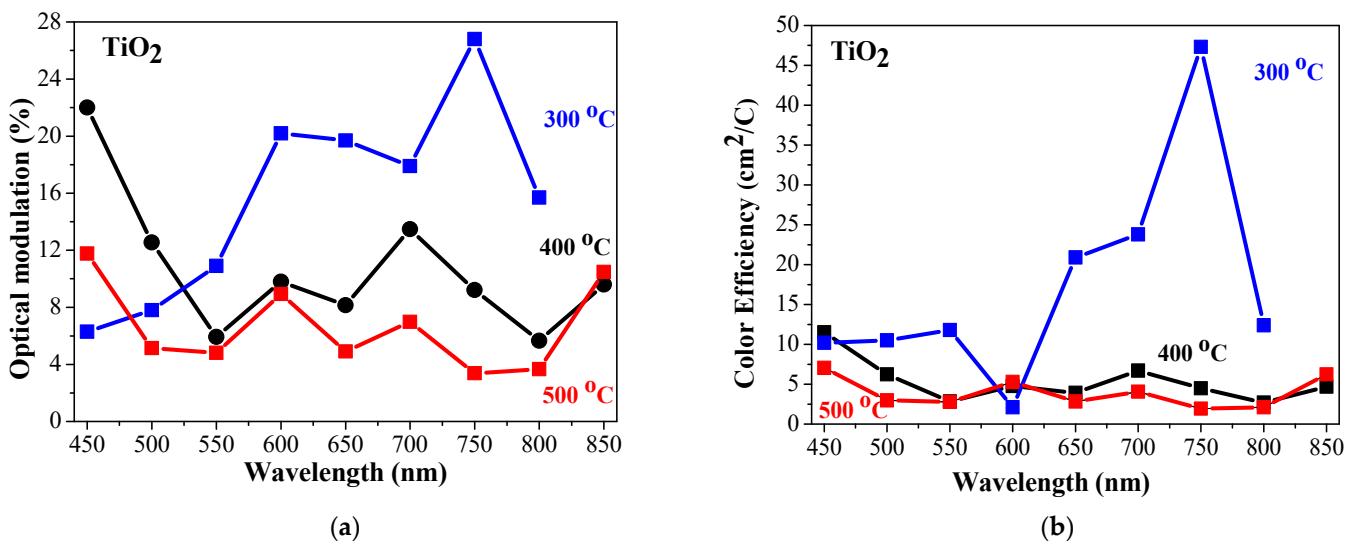


Figure 8. Electrochromic characteristics of sol-gel TiO₂ films annealed at 300, 400 and 500 °C, where (a) presents the optical modulation and (b) color efficiency values.

The electrochromic characteristics significantly decreased for films annealed at higher temperatures. After thermal treatment at 500 °C, the sol-gel TiO₂ films show very low ΔT and CE , indicating that their electrochromic properties worsen. As shown above, the optical transparency of the annealed film is also rapidly decreased (Figure 3).

The optical modulation, ΔT , and the color efficiency, CE , of the mixed TiO_2 -NiO films annealed at $300\text{ }^\circ\text{C}$ are given in Figure 9 compared with the electrochromic characteristics of the pure TiO_2 films.

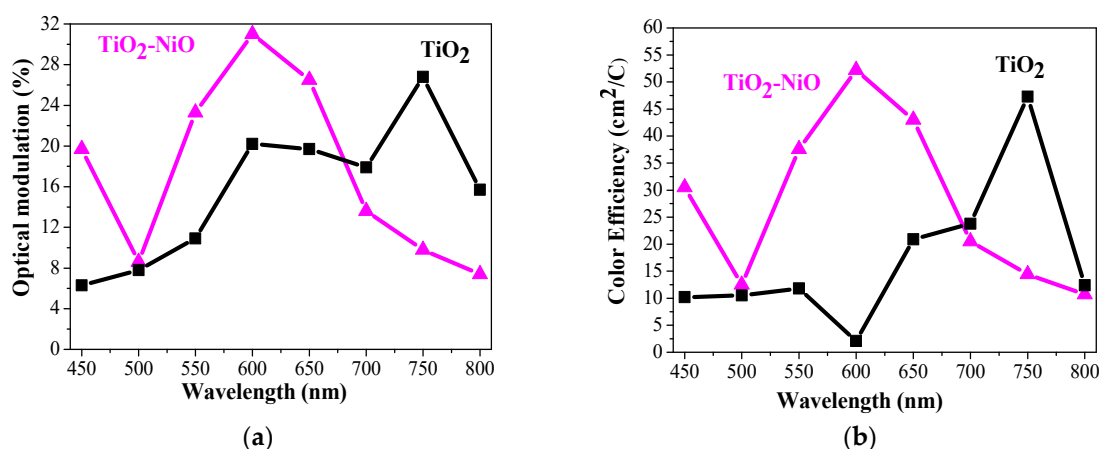


Figure 9. Comparison of (a) the optical modulation and (b) the color efficiency values of sol-gel TiO_2 and TiO_2 -NiO films annealed at $300\text{ }^\circ\text{C}$.

The electrochromic properties of TiO_2 -NiO films are improved, especially for wavelengths of 550, 600 and 650 nm. This is encouraging as it is known that the human eye has the highest sensitivity at a wavelength of 550 nm. For TiO_2 -NiO films, $\Delta T = 23.3$ and 31.0% and $CE = 38$ and $52\text{ cm}^2/\text{C}$ for 550 and 600 nm, respectively. Other authors [69] claim that the sprayed deposited NiO- TiO_2 films show optical modulation (from 48.5 to 27.5%) and color efficiency (123–267 cm^2/C at 600 nm) depending on Ni concentration. It must be noted that the sprayed films are much thicker (over 350 nm).

The cyclic voltametric study of the sol-gel TiO_2 -NiO films annealed at $500\text{ }^\circ\text{C}$ reveals that the intercalation/deintercalation of Li^+ ions is accomplished, but there are only slight changes in film transmittance, supposing that TiO_2 -NiO films annealed at this temperature are optically passive.

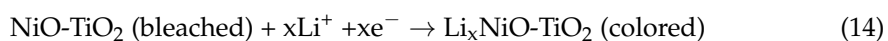
Table 4 presents a comparison of the EC characteristics of the sol-gel deposited TiO_2 and different mixed films from our previous works [70–72]. It can be clearly observed that the mixed system of TiO_2 -NiO possesses the greatest electrochromic characteristics among these investigated thin films.

Table 4. The optical modulation, ΔT , and the color efficiency, CE , of sol-gel TiO_2 and mixed TiO_2 films. The films are annealed at $300\text{ }^\circ\text{C}/1\text{ h}$. The electrochromic characteristics are estimated for $\lambda = 600\text{ nm}$.

	ΔT (%)	CE , (cm^2/C)	Reference
TiO_2	20.21	22.06	This work
TiO_2 -NiO	31.23	52.17	This work
TiO_2 -MnO	19.80	32.30	[70]
TiO_2 - V_2O_5	-	48.3	[71]
TiO_2 - ZrO_2	8.9	12.5	[72]

The possible reason for the improved electrochromic performance of TiO_2 -NiO films is their amorphous-like and disordered structure compared to pure TiO_2 . The amorphous disordered structure of metal oxide thin films favors the electrochromic effect. In the case of the sol-gel TiO_2 and TiO_2 -NiO films, annealing is shown at the lower temperature ($300\text{ }^\circ\text{C}$), where crystallization begins in the presence of the amorphous fraction. The electrochromic characteristics are better than those of well-crystallized samples. It is known that the amorphous electrochromic materials are attractive due to higher atomic

disorder and interstitial spacing. This microstructure may enhance electrochemical cyclic durability [73,74]. For example, other authors [75] found that amorphous sol–gel TiO₂ films have the optimum electrochromic properties. WO₃ is the most studied cathodic electrochromic material and it has been proved that amorphous tungsten oxide favors ion diffusion [9,76]. A recent study [77] reveals that amorphous/crystalline heterostructured WO₃ showed the best EC performance. Their explanation is that the amorphous phase in the amorphous/crystalline heterostructure of the studied film is more loosely packed with a randomly ordered atomic structure, resulting in faster Li ion diffusion and, respectively, better EC properties. Other authors reported that the sol–gel-derived NiO films treated at 300 °C exhibit optimum electrochromic behavior due to their small crystallite sizes and they are more conducive to ion implantation [78]. In this study, it has been found that the diffusion coefficients for Li⁺ ions of mixed Ti-Ni oxide films are higher than those of TiO₂ films. The better electrochromic properties of the composite films can also be influenced by the porosity (see Table 2) and the presence of hydroxyl groups in the film structure (see Figure 2). The hydroxyl ions and water play an important role in the electrochromic mechanism [79]. It is observed that during Li⁺ intercalation/deintercalation, the sol–gel TiO₂ and TiO₂-NiO films show only cathodic-type electrochromism. In the case of mixed oxide films, the following reaction probably takes place [80], similarly to pure TiO₂ (1):



The structural, optical and electrochromic study of the sol–gel composite TiO₂-NiO is promising as there is an improvement in their properties compared to individual metal oxide. Their enhanced electrochromic behavior was determined.

4. Conclusions

Electrochromic thin films of TiO₂ and TiO₂-NiO were deposited on silicon, glass and conductive glass substrates by the sol–gel dip coating method. The XRD study proves that TiO₂ films crystallized in the anatase phase. The structure of the composite TiO₂-NiO films treated at lower annealing temperatures (400 and 500 °C) consisted of the anatase phase, cubic NiO and a small amorphous fraction. After thermal treatment at 600 °C, the appearance of the rhombohedral NiTiO₃ phase in TiO₂-NiO films is established along with anatase, rutile TiO₂ and cubic NiO. FTIR investigation confirms the conclusion of XRD analysis.

Optical characterization reveals that the film transparency of the composite films deteriorates with an increase in the annealing temperature. The direct and indirect optical band gaps of the sol–gel films are determined. The reduced optical band gaps of the mixed Ti-Ni oxide films are associated with the presence of the rutile titania and the nickel titanate fractions in their structure. The refractive index values are within the reported range for TiO₂.

The electrochromic characteristics of TiO₂-NiO films are higher than those of pure titanium dioxide films after low-temperature treatment at 300 °C. The color efficiency values reach 38 (550 nm) and 52 cm²/C (600 nm) and the corresponding optical modulation values reach 23.3 and 31.0%. The best EC characteristics of the sol–gel TiO₂-NiO films are determined in the spectral range 550–650 nm. Meanwhile pure TiO₂ films show their best EC characteristics at wavelengths of 650 and 700 nm. The enhanced electrochromic behavior is suggested to be due to NiO inclusion. The diffusion coefficients are estimated as a function of the scan rates during cyclic voltametric measurements. This research confirms that sol–gel TiO₂ and TiO₂-NiO films have potential as electrochromic and optoelectronic functional materials.

Author Contributions: Conceptualization, A.H. and T.I.; methodology, T.I.; validation, T.K., B.V. and T.I.; formal analysis, A.H.; investigation, T.I., A.H., T.K. and B.V.; data curation, A.H. and B.V.; writing—original draft preparation, T.I.; writing—review and editing, T.I., A.H. and B.V.;

visualization, T.K.; supervision, T.I. All authors have read and agreed to the published version of the manuscript.

Funding: This research paper was funded by the Bulgarian National Science Fund (BNSF) under the project KP-06-N78/7 (5 December 2023).

Data Availability Statement: Data are contained within this article.

Conflicts of Interest: The authors declare no conflicts of interest.

References

1. Shen, S.; Chen, J.; Wang, M.; Sheng, X.; Ghen, X.; Feng, X.; Mao, S.S. Titanium dioxide nanostructures for photoelectrochemical applications. *Prog. Mater. Sci.* **2018**, *98*, 299–385. [[CrossRef](#)]
2. Liboon, A.; Cabo, S.R.; Candidato, R. Physico-Chemical Properties of TiO₂ Coatings Derived from Acid Catalyst-Free Precursor via Spin Coating. *Biointerface Res. Appl. Chem.* **2023**, *13*, 245.
3. Kang, M.; Kim, S.W.; Park, H.Y. Optical properties of TiO₂ thin films with crystal structure. *J. Phys. Chem. Solids* **2018**, *23*, 266–270. [[CrossRef](#)]
4. Kusior, A.; Banas, J.; Trenczek-Zajas, A.; Zubrzycka, P.; Micek-Ilnicka, A.; Radecka, M. Structural properties of TiO₂ nanomaterials. *J. Mol. Struct.* **2018**, *1157*, 327–336. [[CrossRef](#)]
5. Kumi-Barimah, E.; Penhale-Jones, R.; Salimian, A.; Upadhyaya, H.; Hasnath, A.; Jose, G. Phase evolution, morphological, optical and electrical properties of femtosecond pulsed laser deposited TiO₂ thin films. *Sci. Rep.* **2020**, *10*, 10144. [[CrossRef](#)]
6. Ibadurrohman, M.; Hellgardt, K. Morphological Modification of TiO₂ Thin Films as Highly Efficient Photoanodes for Photoelectrochemical Water Splitting. *ACS Appl. Mater. Interfaces* **2015**, *7*, 9088–9097. [[CrossRef](#)]
7. Dhandayuthapani, T.; Sivakumar, R.; Ilangovan, R.; Gopalakrishnan, C.; Sanjeeviraja, C.; Sivanantharaja, A. High coloration efficiency, high reversibility and fast switching response of nebulized spray deposited anatase TiO₂ thin films for electrochromic applications. *Electroch. Acta* **2017**, *255*, 358–368. [[CrossRef](#)]
8. Zhang, B.; Xu, G.; Liu, S.; Chi, F.; Tian, Y. Electrochromic TiO₂ films by a facile solvothermal process: Effect of ethanol content on growth and performance. *Opt. Mater.* **2021**, *122 (Part B)*, 111744. [[CrossRef](#)]
9. Granqvist, C.G. *Handbook of Inorganic Electrochromic Materials*; Elsevier Science: Amsterdam, The Netherlands, 1995.
10. Yuan, J.; Wang, B.; Wang, H.; Chai, Y.; Jin, Y.; Qi, H.; Shao, J. Electrochromic behavior of WO₃ thin films prepared by GLAD. *Appl. Surf. Sci.* **2018**, *447*, 471–478. [[CrossRef](#)]
11. Coşkun, Ö.D.; Atak, G. The effects of lithiation process on the performance of all-solid-state electrochromic devices. *Thin Solid Films* **2018**, *662*, 13–20. [[CrossRef](#)]
12. Granqvist, C.G.; Avendano, E.; Azens, A. Electrochromic coatings and devices: Survey of some recent advances. *Thin Solid Films* **2003**, *442*, 201–211. [[CrossRef](#)]
13. Patel, K.J.; Bhatt, G.G.; Ray, J.R.; Suryavanshi, P.; Panchal, C.J. All-inorganic solid-state electrochromic devices: A review. *J. Solid State Electroch.* **2017**, *21*, 337–347. [[CrossRef](#)]
14. Dinh, N.N.; Oanh NTh, T.; Long, P.D.; Bernard, M.C.; Hugot-Le Goff, A. Electrochromic properties of TiO₂ anatase thin films prepared by a dipping sol-gel method. *Thin Solid Films* **2003**, *423*, 70–76. [[CrossRef](#)]
15. Şilik, E.; Pat, S.; Özen, S.; Mohammadigharehbagh, R.; Yudar, H.H.; Musaoğlu, C.; Korkmaz, Ş. Electrochromic properties of TiO₂ thin films grown by thermionic vacuum arc method. *Thin Solid Films* **2017**, *640*, 27–32. [[CrossRef](#)]
16. Hou, S.; Gavriluk, A.I.; Zhao, Y.; Geng, H.; Li, N.; Hua, C.; Zhang, K.; Li, Y. Controllable crystallinity of nickel oxide film with enhanced electrochromic properties. *Appl. Surf. Sci.* **2018**, *451*, 104–111. [[CrossRef](#)]
17. Zhou, J.; Luo, G.; Wei, Y.; Zheng, J.; Hu, C. Enhanced electrochromic performances and cycle stability of NiO-based thin films via Li-Ti co-doping prepared by sol-gel method. *Electrochim. Acta* **2015**, *186*, 182–191. [[CrossRef](#)]
18. Penin, N.; Rougier, A.; Laffant, L.; Poizot, P.; Tarascon, J.M. Improved cyclability by tungsten addition in electrochromic NiO thin films. *Sol. Energy Mater. Sol. Cells* **2006**, *90*, 422–433. [[CrossRef](#)]
19. Huang, Q.; Zhang, Q.; Xiao, Y.; He, Y.; Diao, X. Improved electrochromic performance of NiO-based thin films by lithium and tantalum co-doping. *J. Alloys Comp.* **2018**, *747*, 416–422. [[CrossRef](#)]
20. Xie, Z.; Liu, Q.; Zhang, Q.; Lu, B.; Zhai, J.; Diao, X. Fast-switching quasi-solid state electrochromic full device based on mesoporous WO₃ and NiO thin films. *Sol. Energy Mater. Sol. Cells* **2019**, *200*, 110017. [[CrossRef](#)]
21. Lee, S.Y.; Lee, T.G.; Nahm, S.; Kim, D.H.; Yang, D.J.; Han, S.H. Investigation of all-solid-state electrochromic devices with durability enhanced tungsten-doped nickel oxide as a counter electrode. *J. Alloys Comp.* **2020**, *815*, 152399. [[CrossRef](#)]
22. Purushothaman, K.K.; Muralidharan, G. The effect of annealing temperature on the electrochromic properties of nanostructured NiO films. *Sol. Energy Mater. Sol. Cells* **2009**, *93*, 1195–1201. [[CrossRef](#)]
23. Passerini, S.; Scrosati, B. Electrochromism of thin-film nickel oxide electrodes. *Solid State Ionics* **1992**, *53–56*, 520–524. [[CrossRef](#)]
24. Atak, G.; Coşkun, Ö.D. Annealing effects of NiO thin films for all-solid-state electrochromic devices. *Solid State Ion.* **2017**, *305*, 43–51. [[CrossRef](#)]

25. Qi, X.; Su, G.; Bo, G.; Cao, L.; Liu, W. Synthesis of NiO and NiO/TiO₂ films with electrochromic and photocatalytic activities. *Surf. Coat. Techn.* **2015**, *272*, 79–85. [[CrossRef](#)]
26. Barmeh, A.; Niliforoushan, M.R.; Otraj, S. Wetting and photocatalytic properties of Ni-doped TiO₂ coating on glazed ceramic tiles under visible light. *Thin Solid Films* **2018**, *666*, 137–142. [[CrossRef](#)]
27. Bo, G.; Wang, X.; Wang, K.; Gao, R.; Dong, B.; Cao, L.; Su, G. Preparation and electrochromic performance of NiO/TiO₂ nanorod composite film. *J. Alloys Comp.* **2017**, *728*, 878–886. [[CrossRef](#)]
28. Green, S.V.; Granqvist, C.G.; Niklasson, G.A. Structure and optical properties of electrochromic tungsten-containing nickel oxide films. *Sol. Energy Mater. Sol. Cells* **2014**, *126*, 248–259. [[CrossRef](#)]
29. Green, S.V.; Pehlivan, E.; Granqvist, C.G.; Niklasson, G.A. Electrochromism in sputter deposited nickel-containing tungsten oxide films. *Sol. Energy Mater. Sol. Cells* **2012**, *99*, 339–344. [[CrossRef](#)]
30. Lee, S.H.; Joo, S.K. Electrochromic behavior of Ni-W oxide electrodes. *Sol. Energy Mater. Sol. Cells* **1995**, *39*, 155–166. [[CrossRef](#)]
31. Al Kahlout, A.; Heusing, S.; Aegerter, M.A. Electrochromism of NiO-TiO₂ sol gel layers. *J. Sol Gel Sci. Tech.* **2006**, *39*, 195–206. [[CrossRef](#)]
32. Harizanov, O.; Harizanova, A. Development and investigation of sol–gel solutions for the formation of TiO₂ coatings. *Sol. Energy Mater. Sol. Cells* **2000**, *63*, 185–195. [[CrossRef](#)]
33. Wen, T.; Niklasson, G.A.; Granqvist, C.G. Electrochromic nickel oxide films and their compatibility with potassium hydroxide and lithium perchlorate in propylene carbonate: Optical, electrochemical and stress-related properties. *Thin Solid Film.* **2014**, *565*, 128–135. [[CrossRef](#)]
34. Mohammadi, M.R.; Fray, D.J. Mesoporous and nanocrystalline sol–gel derived NiTiO₃ at the low temperature: Controlling the structure, size and surface area by Ni:Ti molar ratio. *Solid State Sci.* **2010**, *12*, 1629–1640. [[CrossRef](#)]
35. Pavithra, C.; Madhuri, W. Electrical and magnetic properties of NiTiO₃ nanoparticles synthesized by the sol-gel synthesis method and microwave sintering. *Mater. Chem. Phys.* **2018**, *211*, 144–149. [[CrossRef](#)]
36. Tursun, R.; Su, Y.; Yu, Q.; Tan, J. Room-temperature coexistence of electric and magnetic orders in NiTiO₃ and effect of ethylene glycol. *Mater. Sci. Engin. B* **2018**, *228*, 96–102. [[CrossRef](#)]
37. Xin, C.; Wang, Y.; Sui, Y.; Wang, Y.; Wang, X.; Zhao, K.; Liu, Z.; Li, B.; Liu, X. Electronic, magnetic and multiferroic properties of magnetoelectric NiTiO₃. *J. Alloys Comp.* **2014**, *613*, 401–406. [[CrossRef](#)]
38. Praveen, P.; Viruthagiri, G.; Mugundan, S.; Shanmugam, N. Structural, optical and morphological analyses of pristine titanium di-oxide nanoparticles—Synthesized via sol–gel route. *Spectroch. Acta Part A* **2014**, *117*, 622–629. [[CrossRef](#)]
39. Kaur, G.; Negi, P.; Kaur, M.; Sharma, R.; Konwar, R.J.; Mahajan, A. Morpho-structural and opto-electrical properties of chemically tuned nanostructured TiO₂. *Ceram. Int.* **2018**, *44*, 18484–18490. [[CrossRef](#)]
40. Ranjbar, S.; Saberyan, K.; Parsayan, F. A new process for preparation of Zr doped TiO₂ nanopowders using APCVS method. *Mater. Chem. Phys.* **2018**, *214*, 337–347. [[CrossRef](#)]
41. Vuk, Š.; Ješe, R.; Orel, B.; Dražić, G. The effect of surface hydroxyl groups on the adsorption properties of nanocrystalline TiO₂ films. *Int. J. Photoenergy* **2005**, *07*, 163–168. [[CrossRef](#)]
42. Jiang, K.; Pham, T.T.; Kang, S.G.; Men, Y.; Shin, E.W. Modification of the structural properties of NiTiO₃ materials by transition metal dopants: The dopant size effect. *J. Alloys Comp.* **2018**, *739*, 393–400. [[CrossRef](#)]
43. Singh, P.K.; Mukherjee, S.; Ghosh, K.C.; Maitra, S. Spectroscopic Investigation on Sol Gel Derived TiO₂ Nanoparticles. *J. Adv. Nanomater.* **2017**, *2*, 160–168. [[CrossRef](#)]
44. Rahdar, A.; Aliahmad, M.; Azizi, Y. NiO Nanoparticles: Synthesis and Characterization. *J. Nanostr.* **2015**, *5*, 145–151.
45. Yuvaraj, S.; Nithya, V.D.; Fathima, K.S.; Sanjeeviraja, C.; Selvan, G.K.; Arumugam, S.; Selvan, R.K. Investigations on the temperature dependent electrical and magnetic properties of NiTiO₃ by molten salt synthesis. *Mater. Res. Bull.* **2013**, *48*, 1110–1116. [[CrossRef](#)]
46. Saber, N.B.; Mezni, A.; Alrooqi, A.; Altalhi, T. Enhancement of photocatalytic activity using ternary Au@Pt-TiO₂/nano-GO heterojunction for environmental remediation and clean energy production. *Mater. Res. Exp.* **2021**, *8*, 045014. [[CrossRef](#)]
47. Chellasamy, V.; Thangadurai, P. Structural and electrochemical investigations of nanostructured NiTiO₃ in acidic environment. *Front. Mater. Sci.* **2017**, *11*, 162–170. [[CrossRef](#)]
48. Paul, T.C.; Podder, J.; Paik, L. Effect of Fe doping on the microstructure, optical and dispersion energy characteristics of TiO₂ thin films prepared via spray pyrolysis technique. *Results Opt.* **2022**, *8*, 100235. [[CrossRef](#)]
49. Ghrairi, N.; Bouaicha, M. Structural, morphological, and optical properties of TiO₂ thin films synthesized by the electro phoretic deposition technique. *Nanosci. Res. Lett.* **2012**, *7*, 357. [[CrossRef](#)]
50. Janitabar-Darzi, S.; Mahjoub, A.R.; Nilchi, A. Investigation of structural, optical and photocatalytic properties of mesoporous TiO₂ thin film synthesized by sol–gel templating technique. *Physica E* **2009**, *42*, 176–181. [[CrossRef](#)]
51. Blanco, E.; Domínguez, M.; González-Leal, J.M.; Márquez, E.; Outón, J.; Ramírez-del-Solar, M. Insights into the annealing process of sol-gel TiO₂ films leading to anatase development: The interrelationship between microstructure and optical properties. *Appl. Surf. Sci.* **2018**, *439*, 736–748. [[CrossRef](#)]
52. Ivanova, T.; Harizanova, A.; Surtchev, M.; Nenova, Z. Investigation of sol–gel derived thin films of titanium dioxide doped with vanadium oxide. *Sol. Energy Mater Sol. Cells* **2003**, *76*, 591–598. [[CrossRef](#)]

53. Mathews, N.R.; Morales, E.R.; Cortes-Jacome, M.A.; Antonio, J.A.T. TiO₂ thin films—Influence of annealing temperature on structural, optical and photocatalytic properties. *Sol. Energy* **2009**, *83*, 1499–1508. [[CrossRef](#)]
54. Welte, A.; Waldauf, C.; Brabec, C.; Wellmann, P.J. Application of optical absorbance for the investigation of electronic and structural properties of sol–gel processed TiO₂ films. *Thin Solid Film.* **2008**, *516*, 7256–7259. [[CrossRef](#)]
55. Moghiminia Sh Farsi, H.; Raissi, H. Comparative optical and electrochemical studies of nanostructured NiTiO₃ and NiTiO₃-TiO₂ prepared by a low temperature modified Sol-Gel route. *Electroch. Acta* **2014**, *132*, 512–523. [[CrossRef](#)]
56. Beenkumari, K.S. Synthesis and characterisation of nano-sized nickel titanate photocatalyst. *J. Exper. Nanosci.* **2013**, *8*, 203–209. [[CrossRef](#)]
57. Hung, P.P.; Dung, D.D.; Tuan, N.H.; Trung, N.N.; Bac, L.H. Iron induced room temperature ferromagnetism in ilmenite NiTiO₃ materials. *Mater. Lett.* **2017**, *209*, 284–286. [[CrossRef](#)]
58. Bellam, J.B.; Ruiz-Preciado, M.A.; Edely, M.; Szade, J.; Jouanneaux, A.; Kassiba, A.H. Visible-light photocatalytic activity of nitrogen-doped NiTiO₃ thin films prepared by a co-sputtering process. *RCA Adv.* **2015**, *5*, 10551–10559. [[CrossRef](#)]
59. Hassanien, A.S.; Akl, A.A. Optical characterizations and refractive index dispersion parameters of annealed TiO₂ thin films synthesized by RF-sputtering technique at different flow rates of the reactive oxygen gas. *Phys. B Cond. Matt.* **2020**, *576*, 411718. [[CrossRef](#)]
60. Sta, I.; Jlassi, M.; Hajji, M.; Boujmil, M.F.; Jerbi, R.; Kandyla, M.; Kompitsas, M.; Ezzaouia, H. Structural and optical properties of TiO₂ thin films prepared by spin coating. *J. Sol-Gel Sci. Technol.* **2014**, *72*, 421–427. [[CrossRef](#)]
61. Abdellatif, S.; Sharifi, P.; Kirah, K.; Ghannam, R.; Khalil, A.S.G.; Erni, D.; Marlow, F. Refractive index and scattering of porous TiO₂ films. *Microp. Mesop. Mater.* **2018**, *264*, 84–91. [[CrossRef](#)]
62. Kabir, I.I.; Sheppard, L.R.; Shamiri, R.; Koshy, P.; Liu, R.; Joe, W.; Sorrell, C.C. Contamination of TiO₂ thin films spin coated on borosilicate and rutile substrates. *J. Mater. Sci.* **2020**, *55*, 3774–3794. [[CrossRef](#)]
63. Ukoba, K.O.; Eloka-Eboka, A.C.; Inambao, F.L. Review of nanostructured NiO thin film deposition using the spray pyrolysis technique. *Renew. Sust. Energ. Rev.* **2018**, *82*, 2900–2915. [[CrossRef](#)]
64. Ghodsi, F.E.; Khayatiyan, S.A. Preparation and determination of optical properties of NiO thin films, deposited by dip coating. *Surf. Rev. Lett.* **2007**, *14*, 219–224. [[CrossRef](#)]
65. Bratvold, J.E.; Fjellatg, H.; Nilsen, O. Atomic Layer Deposition of oriented nickel titanate (NiTiO₃). *Appl. Surf. Sci.* **2014**, *311*, 478–483. [[CrossRef](#)]
66. Khalifa, Z.S.; Lin, H.; Shah, S.I. Structural and electrochromic properties of TiO₂ thin films prepared by metallorganic chemical vapor deposition. *Thin Solid Film.* **2010**, *518*, 5457–5462. [[CrossRef](#)]
67. Lindström, H.; Södergren, S.; Solbrand, A.; Rensmo, H.; Hjelm, J.; Hagfeldt, A.; Lindquist, S.E. Li⁺ Ion Insertion in TiO₂ (Anatase), Chronoamperometry on CVD Films and Nanoporous Films. *J. Phys. Chem. B* **1997**, *101*, 7710–7716. [[CrossRef](#)]
68. Verma, A.; Kar, M.; Agnihorty, S.A. Aging effect of diethanolamine stabilized sol on different properties of TiO₂ films: Electrochromic applications. *Sol. Energy Mater. Sol. Cells* **2007**, *91*, 1305–1312. [[CrossRef](#)]
69. Dhandayuthapani, T.; Sivakumar, R.; Ilangovan, R.; Sanjeeviraja, C.; Jeyadheepan, K.; Gopalakrishnan, C.; Sivaprakash, P.; Arumugam, S. Brown coloration and electrochromic properties of nickel doped TiO₂ thin films deposited by nebulized spray pyrolysis technique. *Thin Solid Films* **2020**, *694*, 137754. [[CrossRef](#)]
70. Ivanova, T.; Harizanova, A.; Koutzarova, T.; Vetryuyen, B. Electrochromic and optical study of sol-gel TiO₂-MnO films. *J. Phys. Conf. Ser.* **2020**, *1492*, 012028. [[CrossRef](#)]
71. Ivanova, T.; Harizanova, A. Electrochromic investigation of sol-gel-derived thin films of TiO₂-V₂O₅. *Mater. Res. Bull.* **2005**, *40*, 411–419. [[CrossRef](#)]
72. Ivanova, T.; Harizanova, A.; Koutzarova, T.; Krins, N.; Vetryuyen, B. Electrochromic TiO₂, ZrO₂ and TiO₂-ZrO₂ thin films by dip-coating method. *Mater. Sci. Eng. B.* **2009**, *165*, 212–216. [[CrossRef](#)]
73. Morales-Luna, M.; Arvizu, M.A.; Granqvist, C.G.; Niklasson, G.A. Electrochromic properties of W_{1-x-y}Ni_xTi_yO₃ thin films made by DC magnetron sputtering. *Thin Solid Films* **2016**, *615*, 292–299. [[CrossRef](#)]
74. Gillaspie, D.T.; Tenent, R.C.; Dillon, A.C. Metal-oxide films for electrochromic applications: Present technology and future directions. *J. Mater. Chem.* **2010**, *10*, 9585–9592. [[CrossRef](#)]
75. Wang, C.M.; Lin, S.Y.; Chen, Y.C. Electrochromic properties of TiO₂ thin films prepared by chemical solution deposition method. *J. Phys. Chem. Solids* **2008**, *69*, 451–455. [[CrossRef](#)]
76. Yu, H.; Guo, J.; Wang, C.; Zhang, J.; Liu, J.; Zhong, X.; Dong, G.; Diao, X. High performance in electrochromic amorphous WO_x film with long-term stability and tunable switching times via Al/Li-ions intercalation/deintercalation. *Electroch. Acta* **2019**, *318*, 644–650. [[CrossRef](#)]
77. Kim, H.; Choi, D.; Kim, K.; Chu, W.; Chun, D.M.; Lee, C.S. Effect of particle size and amorphous phase on the electrochromic properties of kinetically deposited WO₃ films. *Sol. Energy Mater. Sol. Cells* **2018**, *177*, 44–50. [[CrossRef](#)]
78. Shi, M.; Qiu, T.; Tang, B.; Zhang, G.; Yao, R.; Xu, W.; Chen, J.; Fu, X.; Ning, H.; Peng, J. Temperature-Controlled Crystal Size of Wide Band Gap Nickel Oxide and Its Application in Electrochromism. *Micromachines* **2021**, *12*, 80. [[CrossRef](#)] [[PubMed](#)]

79. Xia, X.H.; Tu, J.P.; Zhang, J.; Wang, X.L.; Zhang, W.K.; Huang, H. Electrochromic properties of porous NiO thin films prepared by a chemical bath deposition. *Sol. Energ. Mater. Sol. Cells* **2008**, *92*, 628–633. [[CrossRef](#)]
80. Al-Kahlout, A. Electrochromic Properties and Coloration Mechanisms of Sol–Gel NiO–TiO₂ Layers and Devices Built with Them. Ph.D. Thesis, Leibniz-Institute of New Materials-INM and University of Saarland, Saarbruecken, Germany, 2006. Available online: <http://scidok.sulb.uni-saarland.de/volltexte/2006/640> (accessed on 11 July 2006).

Disclaimer/Publisher’s Note: The statements, opinions and data contained in all publications are solely those of the individual author(s) and contributor(s) and not of MDPI and/or the editor(s). MDPI and/or the editor(s) disclaim responsibility for any injury to people or property resulting from any ideas, methods, instructions or products referred to in the content.